Journal of Applied Polymer Science

Synthesis and Characterization of Novel Ultrathin Polyimide Fibers via Sol-Gel Process and Electrospinning

Christian Schramm,[1] Beate Rinderer,[1] Richard Tessadri[2]

[1]Faculty of Chemistry and Pharmacy, Research Institute for Textile Chemistry and Textile Physics, University Innsbruck, Höchsterstrasse 73, A-6850 Dornbirn, Austria

[2]Faculty of Geo- and Atmospheric Sciences, Institute of Mineralogy and Petrography, University Innsbruck, Innrain 52f, A-6020 Innsbruck, Austria

Correspondence to: C. Schramm (E-mail: christian.schramm@uibk.ac.at)

ABSTRACT: Ultrathin polyimide fibers were prepared using the organoalkoxysilanes (3-triethoxysilylpropyl)succinic anhydride (TESPSA) and (3-amino)propyl triethoxysilane (APTES). In the first step, a viscous solution of the corresponding poly(amic) acid (PAA) was produced and electrospun at various high voltages. The fiber diameter distributions of the as-prepared fibers were measured. The thermal imidization at 220°C resulted in the formation of an organic–inorganic hybrid polyimide fiber assembly as shown by FTIR/ATR. Surface morphology was investigated by means of SEM images. TGA measurements made evident that the prepared fibers begin to decompose at 380°C. XRPD pattern of the fibers revealed that a certain ladder-like order exists in the fibers. The water vapor absorption of the thermally (220°C) treated ultrathin polyimide fibers was evaluated. The fiber assemblies treated at 110°C were water soluble, whereas those treated at 220°C were insoluble in water and organic solvents. © 2012 Wiley Periodicals, Inc. J. Appl. Polym. Sci. 000: 000–000, 2012

KEYWORDS: fibers; polyimides; composites

Received 18 June 2012; accepted 15 August 2012; published online
DOI: 10.1002/app.38543

INTRODUCTION

Electrospinning is an excellent technique for the production of continuous fibers with diameters ranging from micrometers to nanometers. The process of electrospinning has several benefits. One attractive feature of electrospinning is the simple and inexpensive setup. A typical apparatus consists of following components: a high-voltage power supply, a spinneret, and an electrically conductive collector. The fibers fabricated possess a high surface to volume ratio. In addition, electrospun nanofibers can be produced from a wide range of polymers that must be soluble in an appropriate solvent.[1–3] The principles of the electrospinning process are as follow: a droplet of the polymer solution is pulled to the capillary tip of the syringe. Owing to the influence of the electrostatic field, the droplet is converted into a conical shape, the so-called Taylor cone. When the electrostatic forces overcome the surface tension, a thin, charged jet stream is ejected and moves to the counter electrode (e.g., copper plate). In the course of this process, the solvent starts to evaporate. As a result, the deposition of ultrathin fibers occurs on a substrate located above the counter electrode.[4–6]

Nanofibrous mats have interconnected pores and a very large surface to volume ratio, which enable such nanofiber assemblies to have many medical and industrial applications. The chemical composition of electrospun mats can also be tailored by using different polymers, polymer blends, or nanocomposites made of organic or inorganic materials. The main application areas are filtration,[7–9] energy storage,[10] tissue engineering scaffolds,[11,12] drug release delivery,[13,14] and smart textiles.[15,16]

The sol–gel process can also be used to produce spinnable polymer solutions, which enable the production of nanofiber materials with novel properties. In the sol–gel chemistry metal and semimetal alkoxides $M(OR)_x$ (e.g., M = Al, Si, Ti, Zr, and Hf) are normally used as precursors. These metal organic compounds have an organic ligand attached to a metal via a metal–oxygen–carbon linkage. Among these precursors the silicon alkoxides $Si(OR)_4$ are those of highest interest. The alkoxy group of the silicon alkoxide hydrolyzes to particles containing Si–OH groups (sol process), which condensate to a three-dimensional siloxane network that is filled with a solvent (gel process).[17–19] The substitution of one alkoxy group by an organic functionality results in the formation of an organotrialkoxysilane $(R^1)_nSi(OR^2)_{4-n}$. The organic group R^1 can consist of various units such as amino, epoxy, glycidoxy, isocyanato, anhydride, mercapto, or vinyl group. Hydrolysis and subsequent condensation of organotrialkoxy-

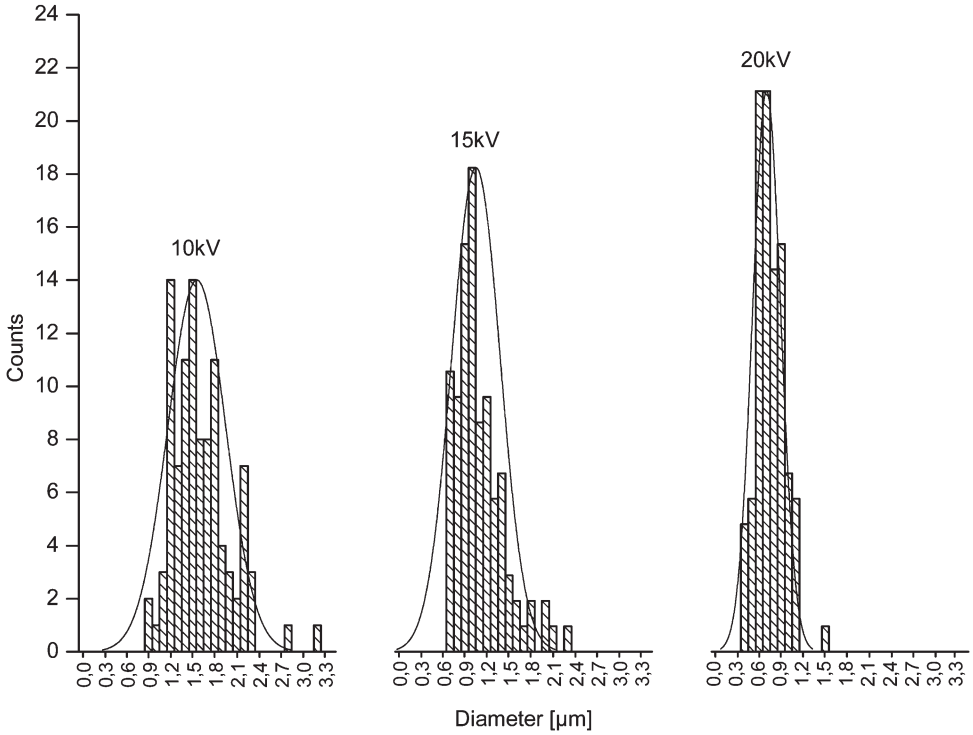

Figure 1. Fiber diameter distribution of TESP-SA/APTES-1/1 (HV: 10, 15, 20 kV, TCD 15 cm).

silanes result in the formation of silsesquioxanes that have the basic repeating unit $[RSiO_{3/2}]$.[20,21]

Polyimides (PI) are a class of polymers possessing the cyclic imide and aromatic groups in the main chain. PI materials are well known for their excellent thermal stability and outstanding properties at elevated temperatures.[22]

Various attempts have been undertaken to synthesize PI nanofibers in order to produce materials with novel properties. Most of the PI-based nanofibers were prepared with pyromellitic dianhydride and 4,4́-oxydianiline. Different additives have been incorporated into the polymer solution to generate nanocomposite ultrathin fiber assemblies.[23–27]

The objective of article is to produce ultrathin, organic–inorganic hybrid PI fibers based on the reaction of (3-triethoxysilylpropyl)succinic anhydride (TESP-SA) and (3-aminopropyl)triethoxysilane (APTES), because previous investigations have shown that hydrolyzed TESP-SA containing two carboxylic groups can react with APTES in the molar ratio of 1: 1 (TESP-SA/APTES-1/1) and of 1 : 2 (TESP-SA/APTES-1/2), thus forming a viscous PAA-solution,[28] which is capable of being subjected to an electrospinning process.

To our knowledge, we produced an ultrathin fiber assembly consisting of a monoimide-bridged polysilsesquioxane for the first time.

EXPERIMENTAL

Materials

TESP-SA and APTES were obtained from Wacker Silicone, Burghausen, Germany. The nonionic surfactant Triton X-100 was supplied by VWR International GmbH, Vienna, Austria. Deionized water (DI) was used throughout the investigations. All reagents were used as received.

The electrospun nanocomposites are denoted as follows: TESP-SA/APTES-molar ratio of mixture–temperature of thermal treatment (e.g., TESP-SA/APTES-1/1-110).

Preparation of the Polymer Solutions

The standard procedure for the synthesis of a TESP-SA/APTES-1/1 sol solution in DI was as follows: TESP-SA (13.96 mL, 50 mmol) were hydrolyzed with HCl (c = 0.05 mol/L, 2.70 mL) in DI (10 mL) under vigorous magnetic stirring (500 rpm) in an open polyethylene beaker (100 mL) for 15 h at room temperature (RT). APTES (11.78 mL, 50 mmol) were added under vigorous stirring. The reaction vessel was covered with a parafilm (Pechiney Plastic Packaging, Chicago, USA) and stirring was continued. After gelation for 24 h at RT, 0.5 mL Triton X-100 were added under constant stirring to improve the spinnability.[29] The concentration %(v/v) of the solution was as follows: TESP-SA 35.8%, HCl (0.05 mol/L) 7.0%, APTES 30.0%, DI 25.8%, Triton X 1.4%.

The electrical conductivity, dynamic viscosity, and surface tension of the as-prepared polymer solutions were measured immediately before being transferred into the syringe.

Apparatus and Methods

The electrospinning apparatus consisted of a syringe pump (Perfusor fm, B. Braun, Melsungen, Germany). A total 5 mL of the polymer solution were fed into a syringe (B/Braun inject, 20 mL), which was placed on the syringe holder. The hypodermic needle (diameter 0.60 mm, length 60 mm) and syringe were connected by means of a plastic tube (Tygon R3607, diameter 1.30 mm, Ismatec, Germany) and appropriate fittings. The feeding rate was

0.1 mL/h. A voltage in the range of 10, 15, and 20 kV, (HV-Quelle, B2electronics, Klaus, Austria) was applied to the needle and after 5 min of electrostatic equilibration the electrospinning experiments were carried out. A rectangular copper collector (25 × 16 cm^2) was tightly wrapped with an aluminum foil and used as counter electrode. The TCD was 15 cm.

The electrical conductivity of the polymer solutions was determined by the aid of a digital conductivity meter LF 537 (WTW, Weilheim, Germany) using the conductivity cell Tetracon 96 (4-electrode system) (WTW, Weilheim, Germany). The viscosity of solutions was measured at 25°C with a Haake Viscotester VT 500 using a MV2 spindle.

To evaluate the surface tension of the polymer solutions, we used a home-built stalagmometer. The surface tension was determined by the drop weight method.[30] DI was used as reference liquid (s = 72.8 mN/m, T = 25°C). The average weights of 50 drops were measured. The surface tension was calculated according to following equation:

$$\sigma_{\text{sample}} = \frac{m_{\text{sample}}/N_{\text{sample}}}{m_{H_2O}/N_{H_2O}} \times \sigma_{H_2O}$$

m = weight of N drops, N = amount of drops

To measure the fiber diameter, the fibers were collected on glass slides. Fiber diameter was determined with an optical microscope Olympus CX41. Statistical calculations were performed with the imaging software Stream (Olympus Soft Imaging Solutions GmbH, Münster, Germany). A minimum of 100 fiber diameters were measured for each sample.

FTIR spectra were recorded with a Bruker Vector 22 spectrometer using a DTGS detector. The spectra were the result of 200 scans. The spectral resolution was 4 cm^{-1}. A PIKE MIRacle™ ATR accessory equipped with a diamond ATR crystal was used for all of the analysis shown in this work.

A Bruker-AXS D8 was used for X-ray powder diffraction (parallel beam optics, Cu-target, energy-dispersive counter, sampler changer with rotation). The samples were run with 40 kV, 40 mA, 2–60° theta/2 theta, 0.01° step size and 5 sec counting time.

SEM micrographs were recorded with an electron microprobe analyzer—JEOL Superprobe 8100. An acceleration voltage of 15 kV was used. The fibers were sputter coated with a layer of gold.

The TGA measurements were conducted with the thermogravimetric analyzer Linseis STA PT1000 (heating rate = 10°C/min; scan range = 40–900°C).

For water vapor adsorption measurements, the specimens were placed in an aluminum dish (diameter: 8 cm, height: 2 cm, the bottom of the dish was replaced by a plastic grid) dried at 105°C and transferred into a desiccator to cool down. First, the weight of the samples was accurately measured. The water vapor adsorption tests were performed gravimetrically by placing the dishes into a desiccator at air humidity 100% at 25°C. The weight of the specimen was measured periodically. The percentage of weight gain was thus calculated as the amount of water vapor adsorption.

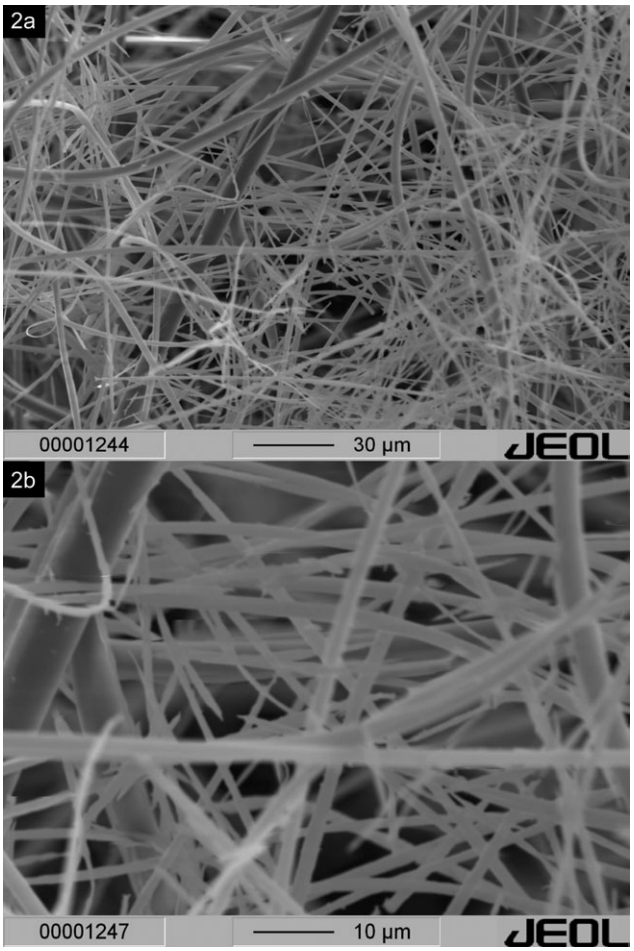

Figure 2. SEM micrographs of TESP-SA/APTES-1/1-220 (a) and TESP-SA/APTES-1/2-220 (b) spun at HV: 15 kV, TCD 15 cm).

RESULTS AND DISCUSSION

The morphology and diameter of electrospun nanofibers depend on various processing parameters: (a) characteristics of the polymer: the type of polymer, the average molecular weight, the conformation of the polymer chain, (b) solvent: the type of solvent, the solvent vapor pressure, the polarity, (c) polymer solution: the polymer concentration, the viscosity, the electrical conductivity, which can be influenced by the addition of salts, the surface tension, (d) the operational conditions: the high voltages (HV) applied, the type of nozzle, the nozzle diameter, the tip-to-collector distance (TCD), the feeding rate, the temperature, and the air humidity. There is a common sense that polymer solution concentration that influences the viscosity, electric field strength, and feeding rate are the main functioning factors.[3,31–34]

Properties of the Polymer Solutions

To produce ultrafine fibers by means of the electrospinning process, the polymer has to be dissolved in an appropriate solvent, as the properties of the polymer solution obtained exert a great influence on the morphology and on the properties of the electrospun fibers. A fiber can only be generated if the electric forces at the surface of the polymer solution droplet overcome

Applied Polymer SCIENCE

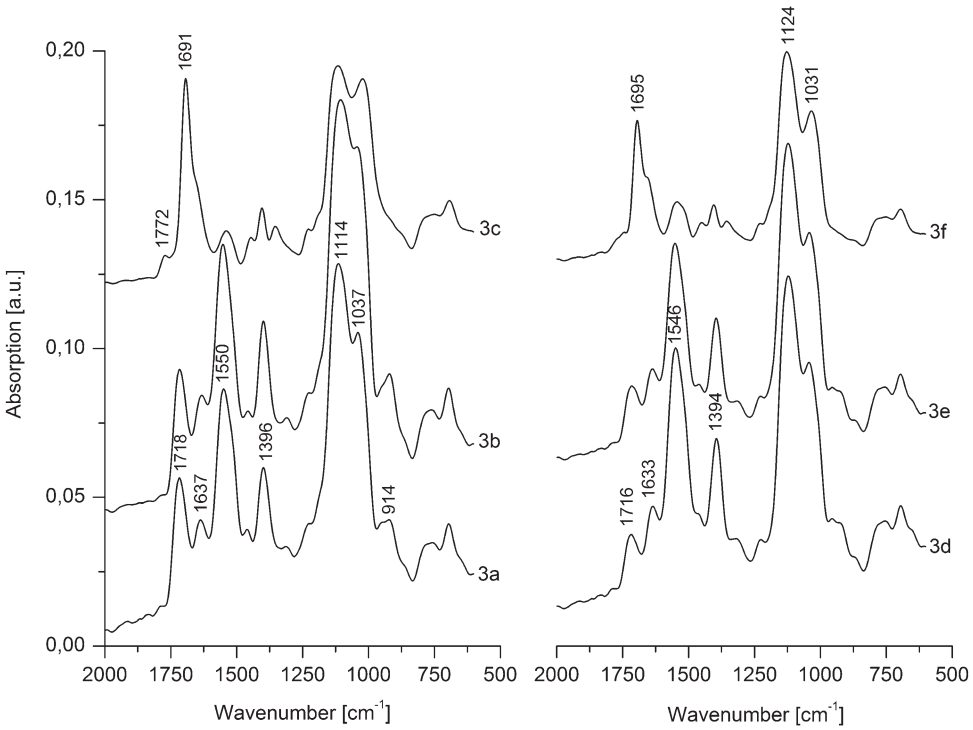

Figure 3. FTIR/ATR spectra of fiber mats TESP-SA/APTES-1/1 (a), TESP-SA/APTES-1/1-110 (b), TESP-SA/APTES-1/1-220 (c) TESP-SA/APTES-1/2 (d), TESP-SA/APTES-1/2-110 (e), and TESP-SA/APTES-1/2-220 (f) indicating that the cyclic polyimide fragment was built, when TESP-SA/APTES-1/1 was treated at 220°C.

the surface tension. As a result, a charged jet can be ejected to the collector. In addition, the polymer solution must also be able to carry sufficient charges; therefore, the electrical conductivity of the polymer solution is of high interest. The viscosity is also a significant parameter. If the viscosity is too low, electrospraying or the formation of beads may occur. If it is too high, the solution cannot be transferred to the top of the needle. Thus, these three parameters have to be optimized.

The surface tension had been modified by adding Triton-X-100. As DI was used as solvent, no alteration of the electrical conductivity was performed.

The polymer was synthesized via the sol–gel process. TESP-SA was hydrolyzed in an acidic solution. The ethoxy groups attached to the silicon atom were converted into hydroxyl groups and the anhydride moiety reacted to the carboxylic groups. The subsequent addition of APTES gave rise to the formation of the poly(amic) acid (PAA). The as-prepared viscous solution was stirred for 2 days and subsequently transferred into the syringe. The prepared polymer solutions were spinnable over a period of 4–5 days.

We measured the viscosity η, the conductivity λ, and the surface tension σ of the polymer solutions: TESP-SA/APTES-1/1 (η = 123.0 mPas, λ = 210 μS/cm, σ = 28.4 mN/m), TESP-SA/APTES-1/2 (η = 144.3 mPas, λ = 212 μS/cm, σ = 26.7 mN/m).

Characterization of the Fibers

The electrospinning process provides nonwoven mats consisting of ultrathin fibers with various diameters. The value of the diameter is affected by several factors. The most crucial issues are the HV and TCD. Thus, we produced fibers applying three HVs (10, 15, and 20 kV). The fibers were collected on a glass slide and dried in a desiccator before the evaluation of the fiber diameter distribution. The results for TESP-SA/APTES-1/1 are shown in Figure 1. The media value decreases as the HV increases. (10 kV: 1.60 ± 0.39 μm; 15 kV: 1.09 ± 0.33 μm, 20 kV: 0.74 ± 0.16 μm). The distribution gets smaller as the HV increases. In the case of TESP-SA/APTES-1/2, the value of the mean diameter does not differ significantly (10 kV: 0.80 ± 0.17 μm; 15 kV: 0.75 ± 0.25 μm; 20 kV: 0.74 ± 0.16 μm). The findings indicate that a wide fiber diameter distribution can be observed. This phenomenon may be due to the fact that the molecular weight of the poly(amic) acid (PAA) built is too low, and therefore, only short polymer chains are present in the electrospinning solution.[35] An increase of the conductivity gives rise to a wider fiber diameter distribution.

Characterization of the Ultrathin Fiber Assemblies

Depending on the spinning time mats with different thicknesses were obtained. The mats were carefully removed from the foil and stored in a desiccator over silica for further investigations.

Figure 2 (a,b) shows the SEM images of TESP-SA/APTES-1/1-220 and TESP-SA/APTES-1/2-220 (HV 15 kV, TCD 15 cm), respectively. The photograph gives evidence that under the spinning condition chosen no beads had been built and fibers with a smooth surface were produced.

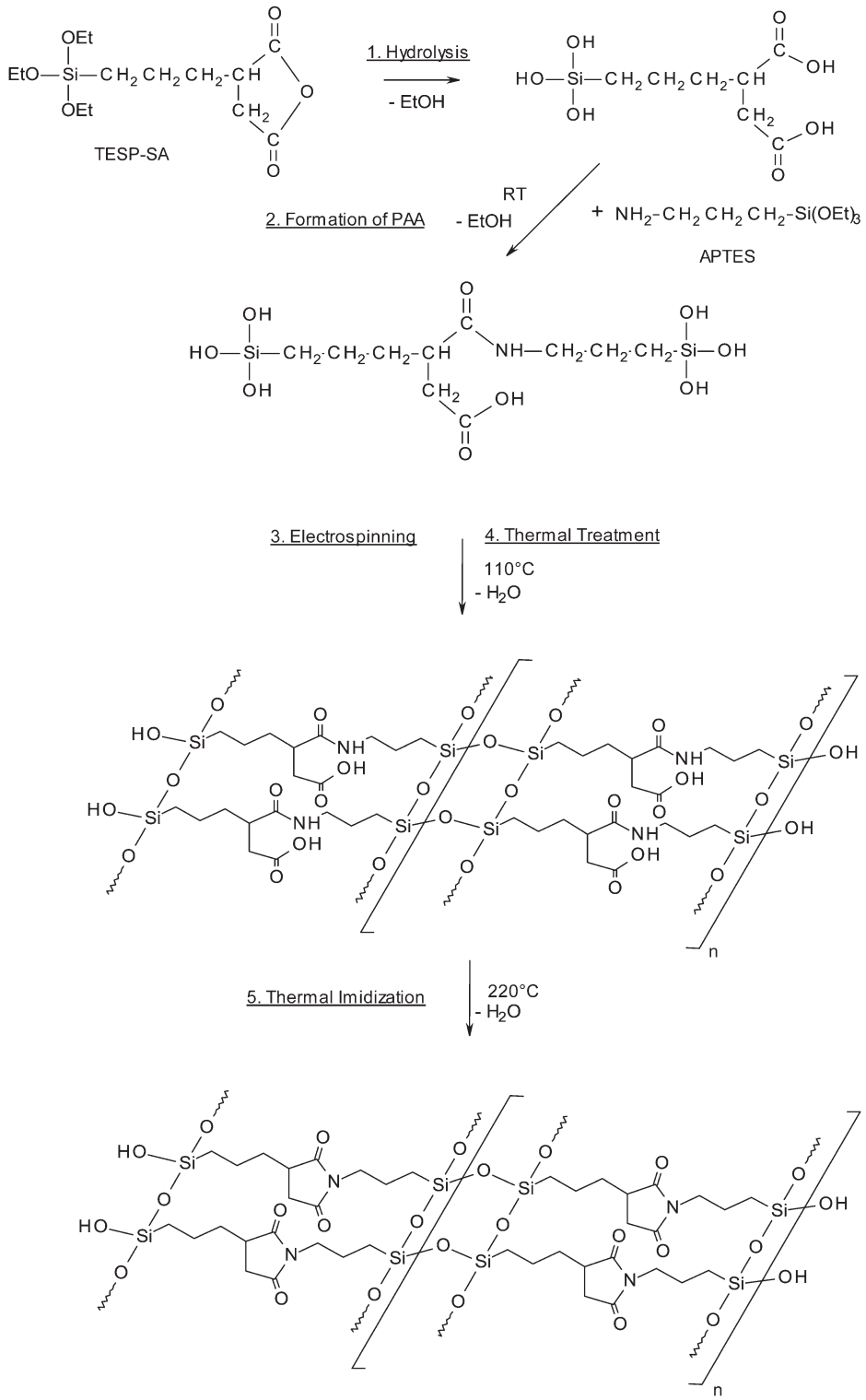

Scheme 1. Formation of the electrospun nanocomposite hybrid PI.

FTIR/ATR

Various studies have shown that FTIR is an excellent analytical method to identify PI-siloxane networks, as the functional groups that are involved in the reaction (carboxylic acids and amides) display intense vibration modes. Also, the imide and cyclic anhydride group formed give rise to several characteristic absorption bands, especially in the carbonyl stretching region.[36–38] Figure 3(a–c) shows the normalized FTIR spectra of the ultrafine fiber assemblies of TESP-SA/APTES-1/1 in the region from 2000 to 600 cm^{-1} (a: dried in a desiccator, b: treated at 110°C for 20 min, c: cured at 220°C for 20 min). No symmetric carbonyl mode of a cyclic anhydride at 1860 cm^{-1} can be seen in the

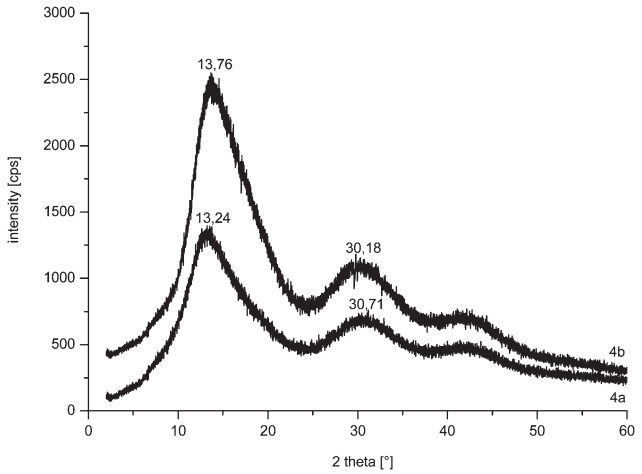

Figure 4. XRPD spectra of TESP-SA/APTES-1/1-220 (a) and TESP-SA/APTES-1/2-220 (b).

spectra in Figure 3a–c. Therefore, it can be concluded that no anhydride moiety was built during the curing process.

No absorption band can be observed at 1770 cm^{-1} (symmetric stretching mode of PI-carbonyl) in the spectrum of TESP-SA/APTES-1/1 [Figure 3(a)] confirming that no PI fragment is formed in the course of the spinning process. The absorption band at 1718 cm^{-1} can be ascribed to the stretching mode of a carboxyl–carbonyl bond. The vibration mode at 1637 cm^{-1} is assigned to the amide I band (stretching mode of the amide carbonyl bond). The amide II band (C—N stretching mode) is observed at 1550 cm^{-1}. The absorption bands at 1396 cm^{-1} are due to the C—H deformation modes of the methylene groups. The bands between 1200 and 1000 cm^{-1} can be attributed to the Si—O—Si modes. The band at 914 cm^{-1} can be assigned to the stretching mode of SiO—H, indicating that the condensation reaction of the SiO—H groups is not driven to completion.

A comparison of Figure 3(b with a) reveals that no significant changes occur when the dried electrospun TESP-SA/APTES-1/1 fiber assembly was subjected to a thermal treatment at 110°C. On the basis of the results from the spectra [Figure 3(a,b)] it can be concluded that PAA was produced.

Figure 3(c) shows the spectrum of TESP-SA/APTES-1/1-220. Two absorption bands at 1772 cm^{-1} and at 1691 cm^{-1} can be observed, which are assigned to the symmetric and the asymmetric carbonyl vibration modes (imide I) of a PI fragment. In addition, one can note that the amide I as well as the amide II band that can be seen in Figure 3(a,b) disappeared.

Figure 3(d–f) shows the normalized FTIR spectra of the ultrafine fiber assemblies of TESP-SA/APTES-1/2 in the region from 2000 to 600 cm^{-1} (3d: dried in a desiccator, 3e: treated at 110°C for 20 min, 3f: cured at 220°C for 20 min). These spectra clearly prove that no imide functionality had been formed, not even when the samples were subjected to a thermal treatment. This phenomenon can be attributed to the fact that no PAA was built under the reaction conditions chosen. It may seem reasonable that the TESP-SA has reacted to a diamide.

These findings indicate that the thermal treatment gives rise to the formation of a PI moiety. Therefore, we suppose that the ultrathin PI fibers are produced according to Scheme 1.

X-Ray Powder Diffraction

Figure 4 depicts the XRPD diffractograms of TESP-SA/APTES-1/1-220 [Figure 4(a)] and TESP-SA/APTES-1/2-220 [Figure 4(b)]. The XRPD pattern show various broad reflection peaks (TESP-SA/APTES-1/1-220: $2\theta = 13.24°$, d_1-spacing: 0.67 nm; $2\theta = 30.18$, d_2-spacing: 0.29 nm; TESP-SA/APTES-1/2-220: $2\theta = 13.76°$, d_1-spacing: 0.64 nm; $2\theta = 30.71$, d_2-spacing: 0.30 nm). Because of the observations of these peaks, it is reasonable to suppose that a certain order exists in the fibers produced. Compared with the findings given in the literature a ladder-like structure can be taken into consideration.[39–41]

Thermogravimetric Analysis

We used TGA to evaluate the thermal behavior of the electrospun organic–inorganic fiber mats.

Figure 5 shows the TGA curves of TESP-SA/APTES-1/1-220 (5a), and TESP-SA/APTES-1/2-220 (5b), indicating that the major weight loss begins at 380°C and can be attributed to the degradation of the organic components of the PI.

Aromatic PIs begin to decompose beyond 480°C.[23,25] The low decomposition temperature can be attributed to the fact that only aliphatic components are present.

To get a better insight into the decomposition mechanism, we have added the corresponding DTG curves of TESP-SA/APTES-1/1-220 (5c), peak temperature (PT) 401°C, and of TESP-SA/APTES-1/2-220 (5d), PT 396°C. The PT indicates the point of greatest rate of change on the weight loss curve. These findings reveal that the thermal properties are almost identical.

Solubility

The fiber assembly consisting of PAA fibers was carefully removed from the aluminum foil and dried in a desiccator. Subsequently, the PAA fiber mat was brought into contact with water. As a consequence, it was completely dissolved. This phenomenon can be explained based on the fact that no formation

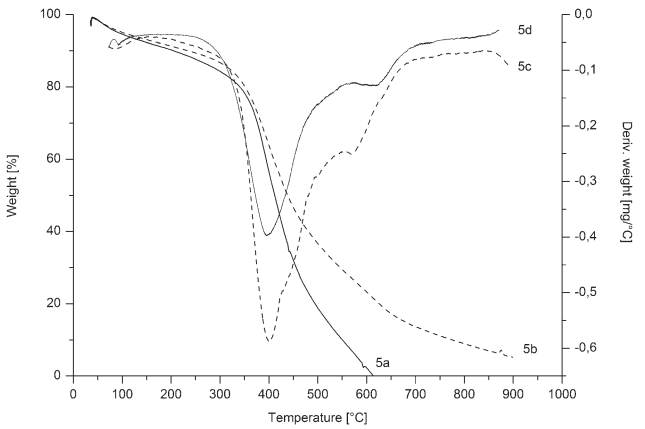

Figure 5. TGA curves of TESP-SA/APTES-1/1-220 (a) and TESP-SA/APTES-1/2-220 (b) and DTG curves of TESP-SA/APTES-1/1-220 (c) and TESP-SA/APTES-1/2-220 (d)

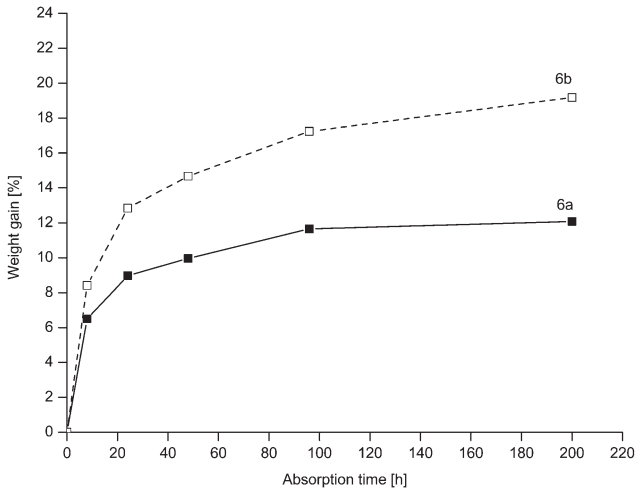

Figure 6. Water vapor absorption (WVA) curves of TESP-SA/APTES-1/1-220 (a) and TESP-SA/APTES-1/2-220 (b).

of siloxane fragments had occurred under the conditions chosen. However, if TESP-SA/APTES-1/1 as well as TESP-SA/APTES-1/2 were treated at 220°C, the as-prepared fiber mats were insoluble in water and in organic solvents, such as tetrahydrofuran and methylene chloride, thus indicating that the thermal treatment at 220°C resulted in the formation of a siloxane-based polymeric network (Scheme 1)

Water Vapor Absorption

An important factor in the selection of a textile material is related to the wearing comfort, which is greatly affected by the ability to absorb or pass water vapor.[42–44] Electrospun assemblies can be sandwiched between two stable textile layers, and thus, significantly improve the comfort features.[45] Therefore, we measured the water vapor absorption (WVA) properties of the ultrathin mats of TESP-SA/APTES-1/1-220 and TESP-SA/APTES-1/2-220, respectively, as the WVA is an indicator of the hydrophobicity of surfaces. The results are shown in Figure 6(a,b), (TESP-SA/APTES-1/1-220) and (TESP-SA/APTES-1/2-220). The findings reveal that TESP-SA/APTES-1/1-220 (24 h, 8%, 97%) has a lower WVA capacity than TESP-SA/APTES-1/2-220 (24 h; 12%, 84%). If polypropylene fibers, which had been modified by means of a super absorbent polymer, were subjected to a WVA test vapor absorption values of 5–8% (24 h) were obtained.[43]

CONCLUSIONS

These results show that an ultrathin fiber based on an organic–inorganic nanocomposite PI can be produced by the sol–gel process and in combination with electrospinning. The first step consists of the hydrolysis of the organoalkoxysilanes TESP-SA. The subsequent addition of APTES results in the formation of a viscous solution of PAA, which can be subjected to an electrospinning process. To produce an ultrathin fiber, it is mandatory to select the proper spinning parameters, especially with respect to the viscosity. The water soluble fibers are treated thermally at 110°C and at 220°C to form water insoluble organic–inorganic nanocomposite fibers. The WVA measurements reveal that TESP-SA/APTES-1/1-220 has a higher hydrophobicity than TESP-SA/APTES-1/2-220.

The very small dimension of these fibers generates a high surface area to volume ratio, which makes them potential candidates for various applications, especially for filtration.

The starting materials have also the advantage of being commercially available and cheap. Further studies must be conducted regarding the optimization of the experimental parameters. The use of other polycarboxylic acids for the production of PI-based ultrathin fibers has to be studied.

ACKNOWLEDGMENTS

The authors would like to thank the Testing Institute of the HTL Dornbirn (Austria) for making available textile-physical devices.

REFERENCES

1. Greiner, A.; Wendorff, J. H. *Angew. Chem-Intern. Edit.* **2007,** *46*, 5670.
2. Li, D.; Xia, Y. N. *Adv. Mater.* **2004,** *16*, 1151.
3. Ramakrishna, S.; Fujihara, K.; Teo Wee, E.; Ma Zu, W. An Introduction to Electrospinning and Nanofibers; World Scientific Publishing Co. Pte. Ltd., Singapore, **2005.**
4. Reneker, D. H.; Chun, I. *Nanotechnology* **1996,** *7*, 216.
5. Reneker, D. H.; Yarin, A. L. *Polymer* **2008,** *49*, 2387.
6. Subbiah, T.; Bhat, G. S.; Tock, R. W.; Parameswaran, S.; Ramkumar, S. S. *J. Appl. Polym. Sci.* **2005,** *96*, 557.
7. Qin, X. H.; Wang, S. Y. *J. Appl. Polym. Sci.* **2008,** *109*, 951.
8. Heikkilä, P.; Taipale, A.; Lehtimäki, M.; Harlin, A. *Polym. Eng. Sci.* **2008,** *48*, 1168.
9. Graham, K.; Ouyang, M.; Raether, T.; Grafe, T.; McDonald, B.; Knauf, P. *Adv. Filtr. Sep. Technol.* **2002,** *15*, 500.
10. Ramakrishna, S.; Jose, R.; Archana, P. S.; Nair, A. S.; Balamurugan, R.; Venugopal, J. R.; Teo Wee, E. *J. Mater. Sci.* **2010,** *45*, 6283.
11. Zhu, X. L.; Cui, W. G.; Li, X. H.; Jin, Y. *Biomacromolecules* **2008,** *9*, 1795.
12. Kumbar, S. G.; James, R.; Nukavarapu, S. P.; Laurencin, C. T. *Biomed. Mater.* **2008,** *3*, 34002/1.
13. Cui, W.; Li, X.; Zhu, X.; Yu, G.; Zhou, S.; Weng, J. *Biomacromolecules* **2006,** *7*, 1623.
14. Venugopal, J.; Prabhakaran, M. P.; Low, S.; Choon, A. T.; Zhang, Y. Z.; Deepika, G.; Ramakrishna, S. *Curr. Pharm. Des.* **2008,** *14*, 2184.
15. Huang, C.; Chen, S.; Reneker, D. H.; Lai, C.; Hou, H. *Adv. Mater.* **2006,** *18*, 668.
16. Bedford, N. M.; Steckl, A. *J. ACS Appl. Mater. Interf.* **2010,** *2*, 2448.
17. Sanchez, C.; Rozes, L.; Ribot, F.; Laberty-Robert, C.; Grosso, D.; Sassoye, C.; Boissiere, C.; Nicole, L. C. R. *Chimie* **2010,** *13*, 3.
18. Corriu, J. P.; Anh, N. T. Molecular Chemistry of Sol-Gel Derived Nanomaterials; John Wiley & Sons Ltd., Chichester, West Sussex, UK, **2009.**

19. Brinker, C. J.; Scherer, G. W. Sol-Gel Science, The Physics and Chemistry of Sol-Gel Processing; Academic Press: San Diego, **1990.**
20. Baney, R. H.; Itoh, M.; Sakakibara, A.; Suzuki, T. *Chem. Rev.* **1995,** *95*, 1409.
21. Shea, K. J.; Loy, D. A. *Chem. Mater.* **2001,** *13*, 3306.
22. Sroog, C. E. *J. Polym. Sci. Part. A: Polym. Phys.* **1967,** *16*, 1191.
23. Zhu, J. H.; Wei, S. Y.; Chen, X. L.; Karki, A. B.; Rutman, D.; Young, D. P.; Guo, Z. H. *J. Phys. Chem. C.* **2010,** *114*, 8844.
24. Nah, C.; Han, S. H.; Lee, M.-H.; Kim, J. S.; Lee, D. S. *Polym. Int.* **2003,** *52*, 429.
25. Cheng, C. Y.; Chen, J.; Chen, F.; Hu, P.; Wu, X. F.; Reneker, D. H.; Hou, H. Q. *J. Appl. Polym. Sci.* **2010,** *116*, 1581.
26. Cheng, S.; Shen, D. Z.; Zhu, X. S.; Tian, X. G.; Zhou, D. Y.; Fan, L. *J. Eur. Polym. J.* **2009,** *45*, 2767.
27. Chen, D.; Liu, T. X.; Zhou, X. P.; Tjiu, W. C.; Hou, H. Q. *J. Phys. Chem. B* **2009,** *113*, 9741.
28. Schramm, C.; Rinderer, B.; Tessadri, R.; Duelli, H. *J. Sol-Gel Sci. Technol.* **2010,** *53*, 579.
29. Wang, S.-Q.; He, J.-H.; Xu, L. *Polym. Int.* **2008,** *57*, 1079.
30. Dilmohamud, B. A.; Seeneevassen, J.; Rughooputh, S. D. D. V.; Ramasami, P. *Eur. J. Phys.* **2005,** *26*, 1079.
31. Andrady, A. L. Science and Technology of Polymer Nanofibers; John Wiley & Sons, Inc, Hoboken, New Jersey, USA, **2008.**
32. Teo, W. E.; Ramakrishna, S. *Nanotechnology* **2006,** *17*, R89.
33. Frenot, A.; Chronakis Ioannis, S. *Curr. Opin. Colloid. Interface Sci.* **2003,** *8*, 64.
34. Megelski, S.; Stephens, J. S.; Chase, D. B.; Rabolt, J. F. *Macromolecules* **2002,** *35*, 8456.
35. Xuyen, N. T.; Ra, E. J.; Geng, H. Z.; Kim, K. K.; An, K. H.; Lee, Y. H. *J. Phys. Chem. B.* **2007,** *111*, 11350.
36. Ahmad, Z.; Al Sagheer, F.; Al Arbash, A.; Ali, A. A. M. *J. Non-Cryst. Sol.* **2009,** *355*, 507.
37. Kurth, D. G.; Bein, T. *Langmuir* **1995,** *11*, 3061.
38. Snyder, R. W.; Thomson, B.; Bartges, B.; Czerniawski, D.; Painter, P. C. *Macromolecules* **1989,** *22*, 4166.
39. Liu, S.; Lang, X.; Ye, H.; Zhang, S. Z. *J. Euro. Polym. J.* **2005,** *41*, 996.
40. Chiang, C. L.; Ma, C. C. M. *J. Polym. Sci. Part A: Polym. Chem.* **2003,** *41*, 1371.
41. Liu, C. Q.; Liu, Y.; Xie, P.; Zhang, R. B.; He, C. B.; Chung, N. T. *React. Funct. Polym.* **2000,** *46*, 175.
42. Eskin, B.; Ucar, N.; Demir, A. *Text Res. J.* **2011**, *81*, 1503.
43. Ucar, N.; Beskisiz, E.; Demir, A. *Text Res. J.* **2009,** *79*, 1539.
44. Lomax, G. R. *J. Mater. Chem.* **2007,** *17*, 2775.
45. Han, X. J.; Huang, Z. M.; He, C. L.; Liu, L.; Wu, O. S. *Polym. Compos.* **2008,** *29*, 579.